





## Benefits of Re-sintering on the Properties of $\text{Al}_2\text{O}_3$ -based Ceramics Obtained by Extrusion 3D Printing

Bruno M. Silva<sup>a</sup> , Joana Baltazar<sup>b</sup>, Ronald P. Cardoso<sup>c</sup> , José Eduardo V. Amarante<sup>d</sup> ,  
Juliana Kelmy Macario Faria Daguano<sup>e</sup>, Claudinei Santos<sup>a,c,\*</sup> 

<sup>a</sup>Universidade Federal Fluminense (UFF), Escola de Engenharia Industrial Metalúrgica de Volta Redonda (EEIMVR), 27255-125, Volta Redonda, RJ, Brasil.

<sup>b</sup>Universidade de Aveiro, Departamento de Engenharia de Materiais e cerâmicos, 3810-193, Aveiro, Portugal.

<sup>c</sup>Universidade do Estado do Rio de Janeiro (UERJ), Faculdade de Tecnologia de Resende (FAT), 27537-000, Resende, RJ, Brasil.

<sup>d</sup>Universidade Federal Fluminense (UFF), Instituto de Saúde de Nova Friburgo (ISNF), 28325-650, Nova Friburgo, RJ, Brasil.

<sup>e</sup>Centro de Tecnologia da Informação Renato Archer (CTI), 13069-901, Campinas, SP, Brasil.

Received: October 29, 2024; Revised: February 07, 2025; Accepted: March 02, 2025

In this study,  $\text{Al}_2\text{O}_3$ -based ceramics were obtained by 3D extrusion printing using an ink containing carboxymethylcellulose (CMC) and polyethyleneimine (PEI) as additives. The ceramic pieces were printed using syringes with nozzles of either 0.25 mm or 0.41 mm diameter at a printing speed of 10 mm/s. After drying, the samples were sintered at 1600 °C for 2 hours and characterized for relative density, microstructure, and crystalline phases. The mechanical properties, including Vickers hardness and fracture toughness, were also evaluated. After sintering, groups of samples were re-sintered at 1610 °C with an isothermal plateau of 0 h, 2 h, or 6 h and then characterized. A group of  $\text{Al}_2\text{O}_3$  samples, the control group, was processed conventionally (uniaxial pressing→sintering at 1600 °C for 2 hours) for comparative analysis. The results indicate that, under all manufacturing conditions,  $\alpha\text{-Al}_2\text{O}_3$  was the only crystalline phase observed. Additionally, the results showed improvements in the mechanical properties of the samples printed by Robocasting after the re-sintering process, regardless of the extrusion nozzle diameter. The relative density increased from 95.3 ±0.4% to 97.4 ±0.3%, Vickers hardness improved from 1322 ±62 HV to 1526 ±45 HV, and fracture toughness increased from 2.3 ±0.4 MPa.m<sup>1/2</sup> to 3.2 ±0.6 MPa.m<sup>1/2</sup>.

**Keywords:** Robocasting,  $\text{Al}_2\text{O}_3$ , ceramic ink, drying behavior, physical characterization, mechanical properties.

### 1. Introduction

Alumina-based ceramics possess a number of favorable properties for various applications, such as high hardness, good wear resistance, excellent chemical stability, and strong thermal stability<sup>1</sup>. These properties enable alumina ( $\text{Al}_2\text{O}_3$ ) to be used as an abrasive material, furnace lining, and components for orthopedic and dental implants, as well as in aerospace applications<sup>2</sup>. Optimization of these properties, particularly the mechanical ones, is achieved by enhancing densification and eliminating porosity during sintering. However, because of the nature of this ceramic's chemical bonds, low sinterability, and microstructural characteristics, eliminating residual porosity proves challenging, which limits its densification.

With advances in technology, the manufacturing industry has become increasingly competitive, necessitating the development of techniques that can achieve the same or even better results – not only at higher speeds but also with

fewer resources. The materials industry is no exception and is similarly striving to develop techniques that meet these demands. Consequently, various studies have been conducted in the field of additive manufacturing to create 3D parts directly from virtual models. These parts are produced by reproducing the models through depositing successive layers of material, with the state or morphology of the material (liquid, powder, paste) determining the applicable techniques. Advances in this field have enabled faster prototyping and the production of more precise parts<sup>3,4</sup>. One of the main advantages of prototyping different components using 3D printing techniques is the rapid construction of components and prototypes, which allows a rapid assessment of their behavior in use in different industrial sectors, generating considerable reductions in the development of new products and thus increasing productivity and competitiveness in the most different sectors of the production chain.

Ceramic robocasting, also known as direct ink writing (DIW), is an additive manufacturing technology based on

\*e-mail: [claudineisvr@gmail.com](mailto:claudineisvr@gmail.com)

material extrusion. In 2000, Cesarano and Calvert<sup>5</sup> developed and patented this technique, which involves the computer-controlled extrusion of a viscous ceramic suspension with a high loading of solids through a small hole, creating filaments that are deposited layer-by-layer<sup>6</sup>. The primary components of ceramic ink used in robocasting processes are an extrudable gel and a filler composed of ceramic powders, which form the basis of the final product. The selection of the ceramic material must align with the desired properties of the final product. The 3D printing technique by robocasting, has some important technological limitations, mainly for the development of dense ceramic parts or those with high dimensional precision. These implications are the result of the low amount of solid charge present in the extruded filaments (usually varying between 30% and 50 vol.%). These characteristics make it difficult to completely eliminate porosity during sintering, as there is a natural distance between the particles, which makes it difficult for the sintering means to act, reducing the final densification. Another factor that limits the use of the technique is the dimensional variation, warping and distortions that occur in 3D printed bodies, due to the difficulty in controlling the drying stage that occurs immediately after printing. In recent years, technological developments have been directed towards environmental control during printing and the respective drying stage, in addition to the optimization of pre-sintering debugging cycles, which allows reducing the problems mentioned above.

Among the different gel compositions used to manufacture ceramic inks for this technique, inks based on carboxymethylcellulose (CMC) and polyethyleneimine (PEI) hydrogel have stood out due to their extrusion-friendly rheology. CMC-PEI gel-based inks exhibit pseudoplastic behavior in other ceramic systems such as 3Y-TZP<sup>7</sup>, as well as the ability to aggregate a large amount of solids, which results in greater green packaging, enabling extrusion through smaller diameter syringe nozzles, thus improving the surface quality of 3D printed parts. In ceramic inks, the presence of carboxymethyl cellulose (CMC) in aqueous alumina suspensions prevented particle agglomeration, reducing viscosity and leading to suspension stabilization<sup>8</sup> through the creation of an electrosteric barrier<sup>8-10</sup>. In addition, Polyethyleneimine (PEI) has a strong coagulant effect, which transforms viscous suspensions into consistent pastes, which allows maintenance of the structural integrity of the filaments after their layer deposition in the DIW process<sup>11,12</sup>. Inks containing alumina ( $\text{Al}_2\text{O}_3$ )<sup>13,14</sup>, zirconia ( $\text{ZrO}_2$ )<sup>15,16</sup>, or  $\text{Al}_2\text{O}_3$ - $\text{ZrO}_2$ <sup>17</sup> or  $\text{ZrO}_2$ - $\text{Al}_2\text{O}_3$ <sup>18</sup> composites have already been investigated, indicating good densification results as well as mechanical properties, which accredits this type of ceramic ink as a natural candidate for future developments in structural parts such as machining tools, for example.

Previous studies have identified the possibility of improving the densification of previously sintered or partially sintered ceramics by applying a re-sintering process. In particular, the re-sintering of alumina-based ceramics,  $\text{Al}_2\text{O}_3$ , was studied to verify the densification and its effects on different properties, as well as on the microstructure of the material. In general, the driving force for increased densification is based on the diffusivity of residual pores that have critical

sizes and shapes<sup>19-23</sup>, motivating an increase in diffusion and the action of densification mechanisms in the final stages of solid phase sintering, in a new round of sintering. Considering that 3D-extrusion techniques allow materials to present both interconnected porosity and residual porosity between particles<sup>7</sup>, since the inks that form the filaments present a relatively low degree of particle packing (green density), of the parts built by 3D printing, there is a window of opportunity for gains in densification, applying a new sintering step, which can be explored in order to identify the gains in densification in return for the grain growth that may eventually occur.

The main objective of this study was the development of alumina-based ceramics obtained by 3D extrusion printing, using a ceramic ink containing 50 wt.%  $\text{Al}_2\text{O}_3$  as solid filler and carboxymethylcellulose (CMC) and polyethyleneimine (PEI) as additives. The material was sintered at 1600°C-2h, and characterized. As a strategy to improve densification, re-sintering combined with isothermal levels was investigated.

## 2. Experimental Procedure

### 2.1. Materials

In this study, a high-purity commercial alumina powder (99.8% purity) containing 0.04% MgO and a specific surface area of 8 m<sup>2</sup>/g (A-1000 Almatis) was used. The average particle size of alumina used in this work was determined in a Laser Scattering Particle Size Distribution Analyzer LA-960, HORIBA. Additionally, carboxymethylcellulose (CMC, 250,000 Mw, Colorobbia, Portugal) was used as a thickening agent for the suspension, along with polyethyleneimine (PEI, Mn ~1800 and Mw ~2000, Sigma-Aldrich, USA), which has a strong coagulating effect, transforming viscous suspensions into solid pastes.

### 2.2. Processing

#### 2.2.1. Preparation of alumina ink ( $\text{Al}_2\text{O}_3$ )

An aqueous suspension of  $\text{Al}_2\text{O}_3$  powder with 50 wt.% solids was prepared by dispersing the alumina powder in deionized water, in the presence of 1 wt.% (based on the amount of alumina solids) of Dolapix CE64 (Zimmer and Schwartz, Germany). This suspension was deagglomerated in a ball mill for 24 hours using alumina balls (3:1 ball-to-powder ratio) to avoid contamination. For the preparation of alumina inks, 0.5 wt.% (based on the amount of alumina solids) of carboxymethylcellulose (CMC, 250,000 Mw, Colorobbia, Portugal) was used as a thickening agent. This binder-assisted suspension was homogenized at 800 rpm in a planetary centrifugal mixer (ARE-250, Thinky Co., Tokyo, Japan) for 5 minutes. Finally, 0.2 wt.% of polyethyleneimine solution (PEI, Mn ~1800 and Mw ~2000, Sigma-Aldrich, USA), was added to obtain extrudable ink with adequate consistency. The final ink was mixed and degassed using the planetary centrifugal mixer again at 1000 rpm for another 5 minutes to ensure homogeneity.

#### 2.2.2. Extrusion - 3D printing

A commercial 3D-extrusion system (Robocasting model EBRD-A32, 3D Inks, LLC, USA) containing the *Robocad*

software (3D inks) was used to print prismatic alumina bars measuring 45 x 4 x 3 mm (length x height x width) using the ink developed in this work, which showed excellent printability in preliminary tests. The ink was loaded into a 5 mL syringe (Nordson, USA) and extruded through nozzles with internal diameters of 0.41 mm and 0.25 mm at a printing speed of 10 mm/s. Printing was conducted at room temperature ( $20 \pm 2$  °C) with controlled 55–60% relative humidity to ensure uniform drying during the procedure. The 3D printing strategy for ceramic parts adopted in this study used “layer by layer” filament deposition, adopting the parallel profiled layer deposition strategy (Angle between layers = 180°), as illustrated in Figure 1 which shows the CAD model of the two different printing configurations used to produce the rectangular samples. The 3D printer programming used the following parameters: 1) center-to-center distance of the filaments = 0.0 mm, 2) Layer height = 0.25 or 0.40 mm, depending on the syringe nozzle used; 3) air gaps between filament deposits = 0.0 mm). After printing, the alumina structures were dried at room temperature with controlled humidity, using a dissector, for 24 hours, followed by drying at 100 °C in an oven for additional 24 hours.

### 2.2.3. Sintering and characterizations

The dried, rectangular bar samples were subjected to dilatometric analysis (DIL 402, Netsch, Germany) under an argon atmosphere using the sintering cycle: 25–600 °C (1 °C/min), 600–1100 °C (2 °C/min). The printed and dried green samples ( $n = 15$  samples per extrusion nozzle) were sintered using an electric furnace (MoSi<sub>2</sub> resistance) (model FE50RPN, FORTELAB, Brazil), following this sintering cycle: room temperature to 300 °C (1 °C/min rate) with a 60-minute step, heating to 600 °C with a new 60-min hold, and heating to 1600 °C (2 °C/min rate) with a 120-minutes hold, followed by controlled cooling (5 °C/min rate).

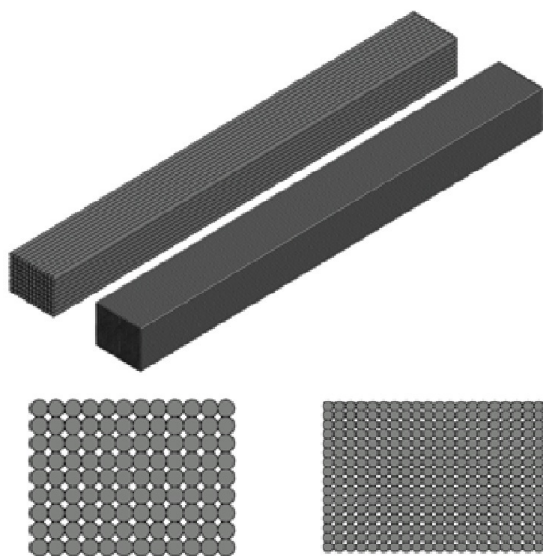


**Figure 1.** Schematic representation of the alumina samples produced by Robocasting; Left: 0.41 mm diameter extrusion nozzle, right: 0.25 mm diameter extrusion nozzle.

All samples obtained by Robocasting and sintered at 1600 °C for 120 minutes were characterized and then re-sintered, in triplicate, at a final temperature of 1610 °C (slightly higher than the original sintering temperature, aiming precisely to achieve re-sintering without high temperature increases that would contribute to probable grain growth), with isothermal thresholds varying between 0, 2, and 4 hours (heating rate of 2 °C/min), to study potential densification increases and investigate possible alumina grain growth.

The apparent density of the sintered samples was measured according to the Archimedes principle<sup>24</sup> Using an OHAUS precision balance (accuracy of 0.0001 g) with specific mass measuring attachments. The relative density values of the samples were calculated using 3.95 g/cm<sup>3</sup><sup>25</sup> as the theoretical density for  $\alpha$ -alumina.

The crystallographic composition of the starting powder and the sintered samples was identified by X-ray diffraction (XRD) using a diffractometer (X'Pert PRO, Malvern Panalytical, Brazil) equipped with a CuK $\alpha$  cathode ray tube ( $\lambda=1.54$  Å). The diffraction spectra were measured over the 20–80° 2 $\theta$  range with an angular step width of 0.01° and an acquisition time of 50 s/step. The crystalline phases were identified by comparison with standard crystallographic data obtained from the PDF-4-ICSD database, using Crystal Match 3.12 software.

The powders as received were analyzed using a Carl ZEISS EVO MA 10 scanning electron microscope (SEM). They were placed on carbon tape and metalized with gold using the Emittech K550X Sputter Coater (Quorum Technologies, Kent, UK). The extruded and sintered samples were analyzed using the TESCAN LYRA3 SEM. The sintered samples underwent metallographic preparation to ready the surfaces for microstructural analysis. The sintered bodies were embedded in cold resin and then ground with 45  $\mu$ m diamond sandpaper using a BUEHLER Ecomet250 automatic polisher. Alumina samples across all studied sintering conditions were ground and polished with diamond suspensions of 9  $\mu$ m, 6  $\mu$ m, 3  $\mu$ m, and finally 1  $\mu$ m. After polishing, the samples were degreased and subjected to thermal etching to reveal the grain boundaries at 1500 °C for 15 minutes, at a heating rate of 20 °C/minute.

### 2.2.4. Mechanical properties

The Vickers hardness of the sintered Al<sub>2</sub>O<sub>3</sub> samples was measured using the Vickers indentation method. At least 20 indentations were made on each sample with an indentation load of 2 kgF (19.8 N) using a microhardness tester (Wilson VH1102, BUEHLER, IL, USA) and DiaMet Template hardness testing software.

Following the proposed methodology, the crack regime was defined based on the relationship between half the distance from the indentation center to the crack tip ( $c$ ) and half the length of the diagonal formed by the indentation ( $a$ ). If  $0.25 \leq c/a \leq 2.5$ , the crack regime is of the Palmqvist-type, and if  $c/a \geq 2.5$ , the crack regime is of the median type.

To analyze the crack system during crack propagation, the model proposed in Equation 1 was selected. The equation, proposed by Casellas<sup>26</sup>, is specific for the Palmqvist crack system and was used in this study.

$$K_{IC} = 0.024 \cdot \left( \frac{E}{HV} \right)^{1/2} \cdot \frac{P}{c^{3/2}} \quad (1)$$

(Palmqvist System,  $0.25 \leq c/a \leq 2.5$ ),

where  $K_{IC}$  is the fracture toughness [ $\text{MPa} \cdot \text{m}^{1/2}$ ],  $E$  is the modulus of elasticity [GPa],  $HV$  is the Vickers hardness [GPa],  $P$  is the indentation load [MPa],  $a$  is the semi-diagonal of the Vickers print [m],  $l$  is the crack length [m];  $c = a + l$ .

### 3. Results and Discussion

#### 3.1. Raw material characterization

Figure 2 shows the results of the characterization of the  $\text{Al}_2\text{O}_3$  powder used in this study. Particles of  $\alpha\text{-Al}_2\text{O}_3$  with an average size close to  $0.6 \mu\text{m}$  were used. The morphological details shown in Figure 2c indicate that the particle system studied is particularly regular, with some agglomerates. The result shown in the diffractogram (Figure 2a) indicates  $\alpha\text{-Al}_2\text{O}_3$  (hexagonal) is the only detectable crystalline phase, confirming that the powder has high crystallinity with intense peaks. Additionally, no other materials were detected that would suggest contamination of the raw material. Figure 2b shows the size distribution analysis of the  $\text{Al}_2\text{O}_3$  particles used in this study, revealing an average size of  $0.58 \pm 0.47 \mu\text{m}$  and a monomodal distribution with some particles smaller than  $0.1 \mu\text{m}$  and larger than  $2 \mu\text{m}$ . These results indicate a moderate range of particle size distribution in the powder. The presence of particles of varying diameters helps to fill the interstices between larger particles, as smaller ones occupy

these gaps. This improves packing and reduces the porosity of the system, Figure 2c provides details of the starting powder's morphology, obtained from SEM micrographs. The micrograph suggests that the commercial powder particles have some agglomerates, in the as-received form, and regular shaped particles with submicron sizes, which was confirmed by particle size analysis, Figure 2b.

#### 3.2. Dilatometry, densification, and crystalline phases

Figure 3 shows the characteristic dilatometry curve of the sample obtained with the  $\text{Al}_2\text{O}_3$ -CMC-PEI ink. The analysis of the shrinkage curve after the dilatometric tests shows a slight change in behavior at temperatures close to  $200^\circ\text{C}$ , which may be associated with the accommodation of the powder particles due to the release of residual molecular water present in the particulate system. This water was not eliminated under the drying conditions imposed during the drying test. Another change in shrinkage behavior is observed around  $700^\circ\text{C}$ , likely related to the evaporation of organic additives present in ink composition. The most pronounced shrinkage, driven by densification mechanisms associated with sintering, begins at temperatures above  $870^\circ\text{C}$  and continues until the test is stopped at  $1100^\circ\text{C}$ , indicating the occurrence of material densification in this region. As the goal of this study was to assess shrinkage during the heating of the ink, the tests were halted at  $1100^\circ\text{C}$ , after which the final densification of the ceramic was achieved.

The results of relative density of sintered samples with different sintering conditions are shown in Figure 4.

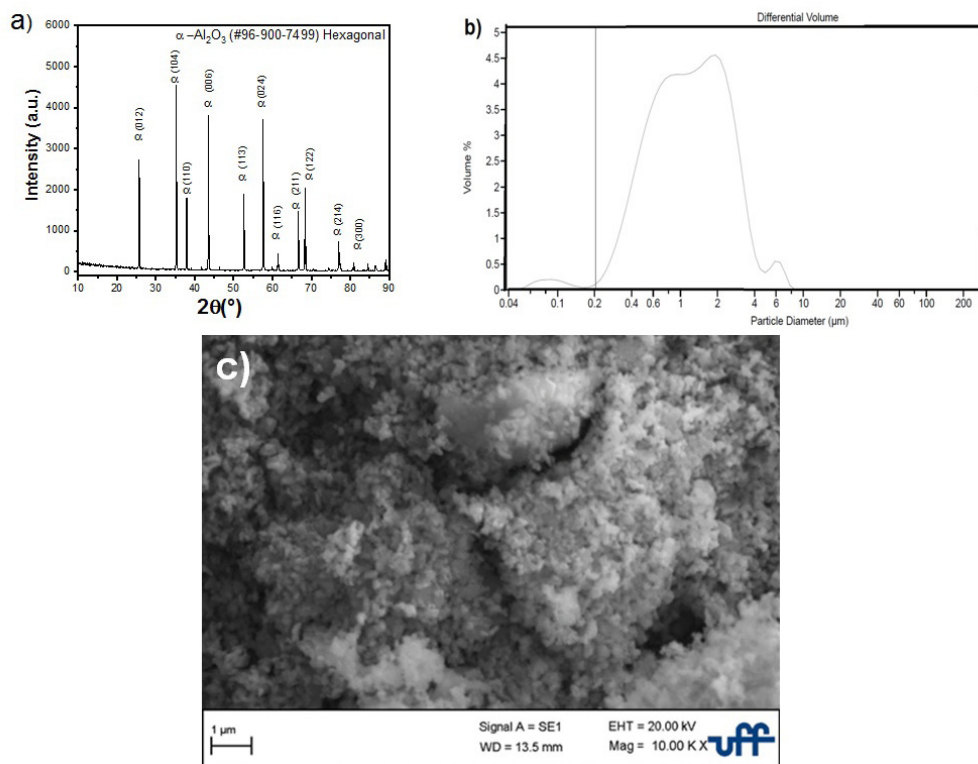


**Figure 2.** a) X-ray diffractogram, b) particle size distribution, and c) micrographs of  $\text{Al}_2\text{O}_3$  starting powder.



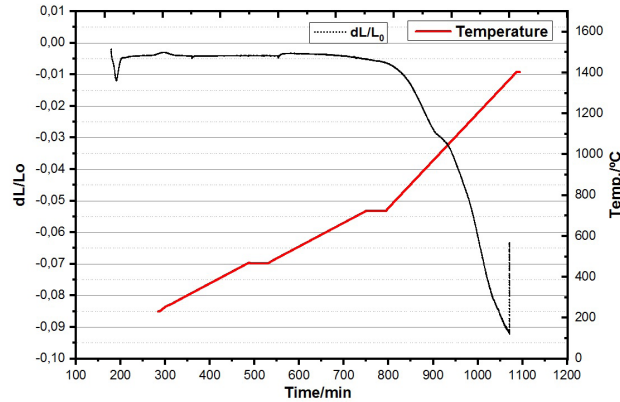


**Figure 3.** Typical dilatometry curve of the extruded material during the initial sintering stage.

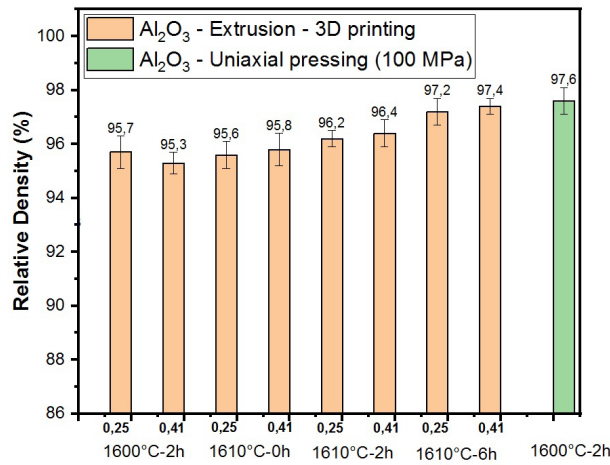


**Figure 4.** Relative density of samples sintered and re-sintered under different conditions: 1600 °C for 2 hours and 1610 °C for 6 hours, respectively. For comparison, the relative density of Al<sub>2</sub>O<sub>3</sub> ceramics sintered at 1600 °C for 2 hours, obtained by compacting, is also shown.

The results of the densification of the samples obtained by Robocasting with the Al<sub>2</sub>O<sub>3</sub>-CMC-PEI ink, indicated that the relative density had average values of  $95.7 \pm 0.6\%$  and  $95.3 \pm 0.4\%$ , when sintered at 1600 °C for 2 hours, for prototypes printed with 0.25 mm and 0.41 mm nozzles, respectively. Therefore, no statistically significant variations were observed in this sintering condition when comparing different printing nozzles. The use of re-sintering (1610°C), as well as the association with isotherm levels, improved the densification of the all groups. Although the relative density values between groups of samples sintered at 1600°C-2h, printed with Ø 0.25mm or Ø 0.41mm nozzles, showed a slight increase in relative density, consistent with the interconnected porosity illustrated in Figure 1, some groups of re-sintered samples showed the opposite behavior, with a small increase in densification for the samples printed with a 0.41mm diameter nozzle, however, within a statistical similarity. In this sense, it is worth noting that, since these are different groups of samples, some 3D printing defect may have occurred, such as microbubbles present in the filaments, not externally noticeable. Furthermore, due to the limited number of samples per sintering condition, it is

not possible to state that there is a tendency for increased densification for larger filaments. The result obtained for the control group (alumina compacted and sintered at 1600°C-2h ( $97.6 \pm 0.5\%$ ), is slightly better than the group of 3D printed samples resintered at 1610°C-6h, due to the better degree of interparticle packing generated in the uniaxial pressing step at 100 MPa.

The sintering condition at 1600 °C for 2 hours indicated that densification was around 96%. The use of re-sintering and additional sintering levels proved effective in improving densification, reaching values of  $97.2 \sim 97.4\%$  when the material was re-sintered at 1610 °C for 6 hours. The reheating process with controlled rates and a higher final temperature, combined with a new isotherm plateau, allowed diffusion events to eliminate pores or reduce pores, contributing to an increase in final densification. Alumina (Al<sub>2</sub>O<sub>3</sub>) is a ceramic material with strong ionic chemical bonds and a high melting temperature, making it difficult to sinter. Thus, the results obtained in this study for materials produced by DIW can be considered encouraging and could be further improved with new sintering strategies, such as hot pressing or sintering at higher temperatures under vacuum.

Figure 5 shows the results of X-ray diffractograms obtained under the extreme sintering conditions applied in this study for the alumina ink samples. The presence of the  $\alpha$ - $\text{Al}_2\text{O}_3$  crystalline phase (hexagonal) is observed as the only crystalline phase present after sintering. This result is consistent with those reported for alumina ceramics produced by conventional compaction and sintering processes<sup>27,28</sup>. The results of the Rietveld refinement are shown in Table 1, indicating stability of the lattice parameters after sintering, even when a new sintering cycle was applied.

3.3. Scanning Electron Microscopy (SEM)

SEM analysis was performed on the samples produced with the  $\text{Al}_2\text{O}_3$ -CMC-PEI ink using extrusion nozzles of different diameters. The results in Figure 6a and 6b highlight the morphology and details of the filament layers. The micrographs of the sintered  $\text{Al}_2\text{O}_3$ -CMC-PEI ink samples produced with Ø 0.25 mm extrusion nozzles (Figure 6a) show interconnected residual porosity, mainly in the filament regions closest to the surface. This behavior is mainly due to the greater drying effect on the initial printing layers compared to the more central layers. Since the drying rate is very fast in the first few minutes of printing, defects are more likely to occur in these regions. This higher drying rate observed during the initial minutes of exposure to air is due to the dynamics of moisture removal during drying<sup>29,30</sup>. Among several reasons for this phenomenon, one can mention the availability of moisture on the surface of the printed sample (ceramic surface saturated with free water, which evaporates rapidly under environmental conditions (temperature, air flow, humidity).

This behavior is also observed in the samples printed with 0.41 mm extrusion nozzles (Figure 6b). Because of the larger filament dimensions, the difference in shrinkage of these filament layers and the total volume of layers can cause more severe defects, which can lead to significant

surface quality losses, affecting the densification and the mechanical properties of the parts produced by Robocasting.

Being aware of this behavior, one could opt to discard these samples or perform a diamond grinding operation on the outermost, more defective layers before using the material. When prototyping parts obtained by Robocasting, it is essential to account for the need for a final finish sintering. SEM micrographs detailing the microstructural aspects of alumina sintered at 1600 °C for 2 hours are shown in Figure 7. As expected, similar microscopic features are observed in Figures 7a and 7b for the groups of samples manufactured using different extrusion nozzles, exhibiting equiaxed alumina grains with an average size of less than 2 µm. The results related to the effects of re-sintering are presented in the following three figures.

3.4. Re-sintering: densification and grain growth

Figure 8 shows SEM micrographs of alumina ceramics re-sintered at 1610 °C with different isothermal times. For grain size distribution analysis, *ImageJ* software was used<sup>31</sup>. Grain size analysis was conducted using the Ferret diameter measurement method. The results of grain quantification using *ImageJ* software are shown in Figure 9.

The microstructural analysis shows that grain growth occurred as a function of the isotherm plateau time, without being influenced by the type of nozzle used for printing. The parts re-sintered at 1610 °C without an isotherm reached an average size of 1.5 µm, while increasing the isotherm at 1610 °C to 6 hours led to an average alumina grain size increase to approximately 2.75 µm. Alumina ceramics present a known difficulty in densification and grain growth when sintered at temperatures below 1600 °C and without a sintering isotherm. The use of re-sintering at a temperature of 1610 °C for periods of up to 6 hours allows the material to be subject to a new round of activation of sintering mechanisms responsible for densification, allowing a small increase in the densification of the material to be observed for longer

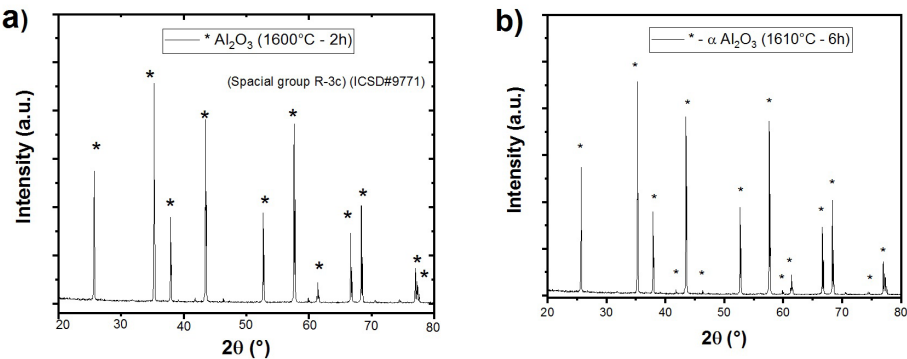
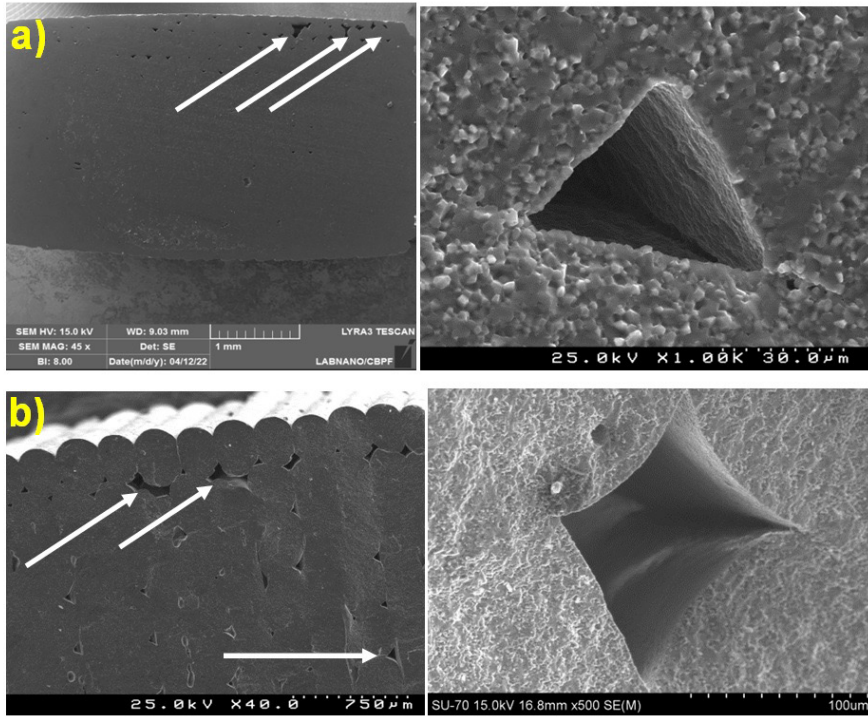


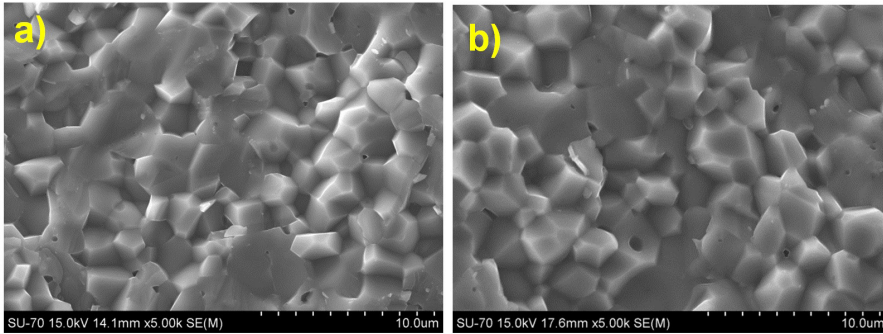
Figure 5. XRD pattern of sintered  $\text{Al}_2\text{O}_3$  ceramic: (a) at 1600 °C for 2 hours and (b) at 1610 °C for 6 hours.

Table 1. Lattice parameters of  $\text{Al}_2\text{O}_3$  samples sintered at different temperatures.

Sample	Identified Phase	lattice parameters (nm)			Vol (nm <sup>3</sup> )	$\chi^2$	Amount (wt.%)
		a	b	c			
1600/2h	$\text{Al}_2\text{O}_3$	4.7594	4.7594	12.9976	294.42	2.20	100
1610/6h		4.7597	4.7597	12.9982	294.47	1.78	100



**Figure 6.** Cross-section of Al<sub>2</sub>O<sub>3</sub> sample obtained by Robocasting, sintered at 1600 °C for 2 hours: a) Ø 0.25 mm extrusion nozzle; b) Ø 0.41 mm extrusion nozzle.



**Figure 7.** a) Microstructure of Al<sub>2</sub>O<sub>3</sub>-CMC-PEI samples sintered at 1600 °C for 2 hours : a) Ø 0.25 mm extrusion nozzle; b) Ø 0.41 mm extrusion nozzle.

sintering times. Furthermore, in these sintering conditions with higher levels at 1610 °C, such as 6 hours, the diffusion mechanisms related to grain growth are predominant, which allows smaller grains in contact with larger grains, and preferably in regions with smaller pores, to undergo an increase in their final size. Thus, the longer sintering times and, consequently, the higher grain boundary diffusion rates under these sintering conditions, are responsible for both a slight increase in densification as well as an increase in the average size of the alumina grains.

Grain size in sintered material is a key factor controlling hardness, fracture toughness, and wear resistance of alumina<sup>32-34</sup>. The importance of using long isotherm plateaus in the sintering of ceramics obtained by Robocasting should be analyzed in conjunction with the benefits of this approach in material densification, especially when aiming for dense materials for structural applications.

### 3.5. Mechanical properties

Table 2 summarizes the properties of the ceramics after sintering. Additionally, Figure 10 presents the Vickers hardness and fracture toughness results of the parts obtained by Robocasting under various sintering conditions.

The samples sintered at 1600 °C - 2h presented Vickers hardness between 1322 HV and 1330 HV, for Ø 0.25 mm and Ø 0.41 mm syringe nozzles, respectively. Comparing the results with samples conventionally compacted and sintered at 1600 °C - 2h (hardness of 1492 HV), values 11 ~ 13% lower than the control group were observed, which is directly related to the densification of the ceramics. After re-sintering at 1610 °C - 6h, the sintering condition where the highest densification was achieved, the average hardness values were 1517 HV (Ø 0.25 mm nozzle) and 1526 HV (Ø 0.41 mm nozzle), indicating that the hardness values are



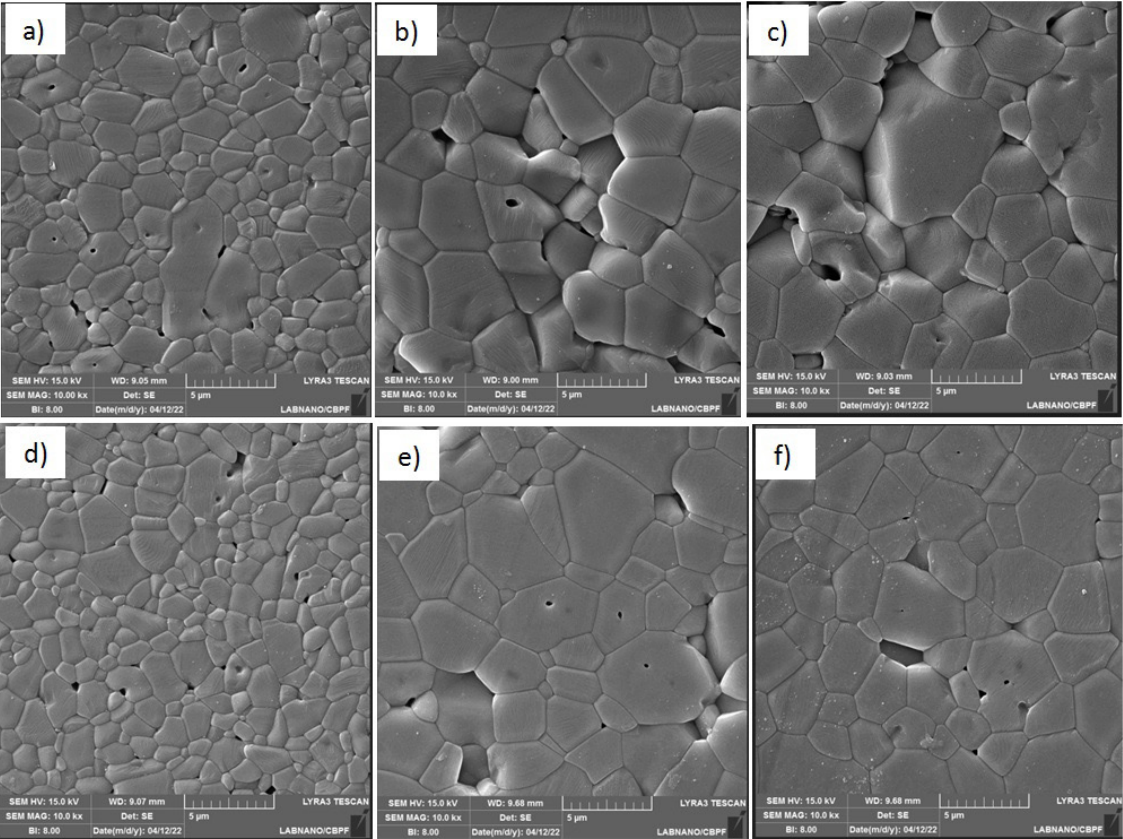


**Figure 8.** SEM micrographs of  $\text{Al}_2\text{O}_3$  ceramics ( $\varnothing$  0.25 mm or  $\varnothing$  0.41 mm extrusion nozzle) obtained by Robocasting and re-sintered at:  $\varnothing$  0.25 mm extrusion nozzle: a) 1610 °C for 0 hours; b) 1610 °C for 2 hours; c) 1610 °C for 6 hours;  $\varnothing$  0.41 mm extrusion nozzle: d) 1610 °C for 0 hours; e) 1610 °C for 2 hours; f) 1610 °C for 6 hours.

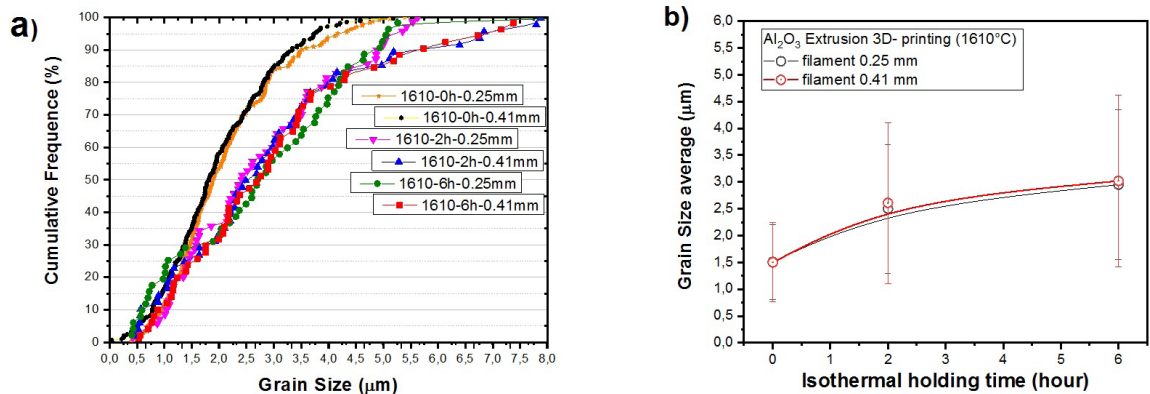


**Figure 9.** a)  $\text{Al}_2\text{O}_3$  grain size distribution curves for the different groups of samples re-sintered under different conditions; b) average  $\text{Al}_2\text{O}_3$  grain size re-sintered at 1610° C as a function of isotherm plateau time.

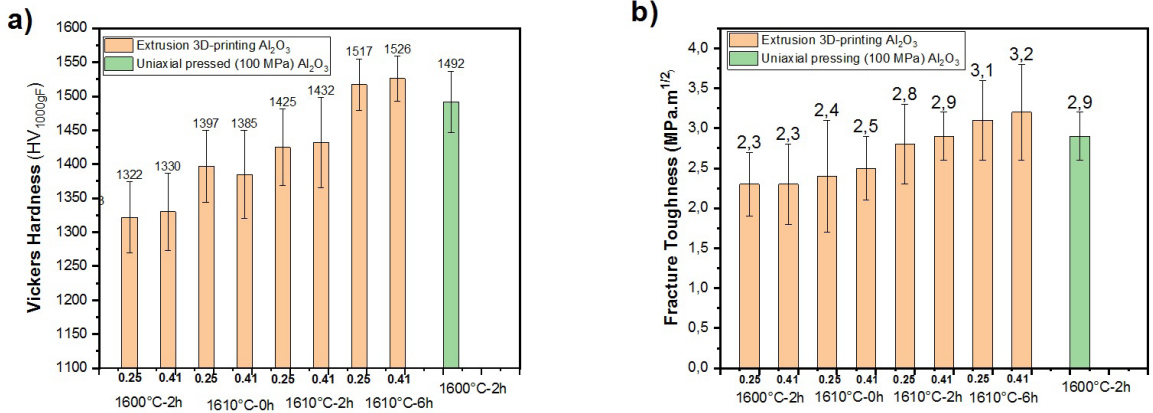
higher and statistically significant in relation to the material sintered at 1600°C-2h. When these re-sintering results are compared to samples conventionally compacted and sintered at 1600 °C - 2h, the results are statistically similar, indicating that re-sintering produces a positive effect on the hardness of ceramics. In terms of fracture toughness, all materials showed statistically similar results within the error range, with a slight advantage for the  $\text{Al}_2\text{O}_3$ -CMC-PEI

inks, as illustrated in Figure 10b. It is worth noting that the technique for determining fracture toughness by Vickers indentation has limitations and imprecision, which must be considered when analyzing these results. Therefore, the results presented here are preliminary in nature and should be proven in future research that integrates the determination of the flexural strength of the material, as well as the determination of fracture toughness by the V-notch method. Regarding



**Table 2.** Mechanical properties of alumina-based ceramics as a function of the printing parameters and sintering cycle used.

Sintering temperature	Material	Ø Extrusion nozzle (mm)	Relative density (%)	Vickers hardness (HV)	Fracture toughness (MPa.m <sup>1/2</sup> )
				HV <sub>(19.8 N)</sub>	
1600 °C – 2 h	Extruded Al <sub>2</sub> O <sub>3</sub> -CMC-PEI	0.25	95.7 ±0.6	1322 ±62	2.3 ±0.4
		0.41	95.3 ±0.4	1330 ±57	2.3 ±0.5
1600 °C – 2 h → 1610 °C – 0 h	Extruded Al <sub>2</sub> O <sub>3</sub> -CMC-PEI	0.25	95.6 ±0.5	1397 ±53	2.4 ±0.7
		0.41	95.8 ±0.6	1385 ±65	2.5 ±0.4
1600 °C – 2 h → 1610 °C – 2 h	Extruded Al <sub>2</sub> O <sub>3</sub> -CMC-PEI	0.25	96.2 ±0.3	1425 ±66	2.8 ±0.5
		0.41	96.4 ±0.5	1432 ±38	2.9 ±0.3
1600 °C – 2 h → 1610 °C – 6 h	Extruded Al <sub>2</sub> O <sub>3</sub> -CMC-PEI	0.25	97.2 ±0.5	1517 ±33	3.1 ±0.5
		0.41	97.4 ±0.3	1526 ±45	3.2 ±0.6
1600 °C – 2 h	Compacted monolithic Al <sub>2</sub> O <sub>3</sub>	---	97.6 ±0.5	1492 ±70	2.9 ±0.3

**Figure 10.** a) Vickers hardness and b) fracture toughness of extruded Al<sub>2</sub>O<sub>3</sub> ceramics sintered at different conditions, and compacted Al<sub>2</sub>O<sub>3</sub> inks sintered at 1600° C - 2 h.

densification (Figure 4), the Al<sub>2</sub>O<sub>3</sub>-CMC-PEI inks showed no significant differences when comparing their results with different extrusion nozzle sizes (Ø 0.25 mm and Ø 0.41 mm).

The re-sintering process at 1610 °C for 6 hours was important in optimizing the mechanical properties of the ceramic materials. By employing a slow heating rate to facilitate the removal of binders and a sintering temperature suitable for ceramic materials, densification increased without significant grain growth. Despite the sintering cycles used in this study, residual porosity remained in the samples, predominately located at the filament junctions. Notably, the Al<sub>2</sub>O<sub>3</sub>-CMC-PEI ink achieved results comparable to, and in some cases better than, uniaxially compacted Al<sub>2</sub>O<sub>3</sub>. The relative density values are in line with those reported in various studies<sup>27,28,34,35</sup>, where values ranging from 92% to 98% were achieved under similar sintering conditions. It is well established that residual porosity significantly influences the mechanical properties of ceramic materials. Therefore, it is suggested that, in future work, studies aimed at advanced debinding techniques and flexural strength evaluation be proposed.

#### 4. Conclusions

The characterizations conducted in this study showed that the Al<sub>2</sub>O<sub>3</sub>-CMC ink with a concentration of 0.5% CMC and the Al<sub>2</sub>O<sub>3</sub>-CMC-PEI ink exhibited rheological properties

suitable for 3D extrusion. The sintering results indicated an increase in relative density during the re-sintering stage, accompanied by a corresponding increase in Al<sub>2</sub>O<sub>3</sub> grain size as the isotherm plateau time increased. Despite the growth of alumina grains, the improvement in densification during re-sintering led to corresponding increases in the hardness and fracture toughness of the ceramic materials. Under the sintering conditions with isothermal thresholds, the densification values were found to be of the same order of magnitude as those obtained using conventional processing techniques (uniaxial pressing at 100 MPa followed by sintering at 1600 °C for 2 hours). This demonstrates the potential of the inks developed with CMC-PEI additives for the manufacture of dense alumina parts with good mechanical properties, comparable to ceramics obtained by conventional alumina processing route (uniaxial pressing→sintering).

#### 5. Acknowledgments

Dr. Claudinei Santos is grateful to the Brazilian agencies FAPERJ (Grant E26-202.997/2017) and CNPq (Grant 311.119/2017-4) for the financial support received.

#### 6. References

1. Southern JC. A review of alumina production, characterization, and use. Materials & equipment/whitewares: ceramic

- engineering and science proceedings. In: Carty WM, editor. Hoboken: John Wiley & Sons; 2001. Chapter 12. <http://doi.org/10.1002/9780470294673.ch12>.
2. Sousa LF, Simba BG, Souza JVC, Ribeiro MV, Silva OMM, Santos C. Dry machining of nodular cast iron using a YAG-reinforced alumina ceramic cutting tool. *Int J Adv Manuf Technol*. 2022;123(1-2):99-110. <http://doi.org/10.1007/s00170-022-10149-8>.
  3. Yang K, Li Q, Chen T, Jin F, Liu X, Liang J, et al. High-performance 3D-printed  $\text{Al}_2\text{O}_3$  cores for low-temperature sintering. *Ceram Int*. 2023;49(22):36894-906. <http://doi.org/10.1016/j.ceramint.2023.09.020>.
  4. Minatti J, Santana J, Fernandes R, Campos E. Alumina developed by pre gelling starch consolidation (PSC). *J Eur Ceram Soc*. 2009;29(4):661-8. <http://doi.org/10.1016/j.jeurceramsoc.2008.07.046>.
  5. Cesarano J, Calvert PD. Freeforming objects with low-binder slurry. United States patent US 6027326A. 2000, Feb. 22.
  6. Daguano JKMB, Santos C, Souza MTT, Alves MFRP, Fernandes MHFV, Silva JVL. State of the Art in the use of bioceramics to elaborate 3D structures using robocasting. *Int J Adv Med Biotechnol*. 2019;2(1):55-70. <http://doi.org/10.25061/2595-3931/IJAMB/2019.v2i1.28>.
  7. Baltazar J, Alves MFRP, Martins MA, Torres PMC, Santos C, Olhero S. Flexural strength of 3Y-TZP bioceramics obtained by direct write assembly as function of residual connected-porosity. *J Mech Behav Biomed Mater*. 2022;126:105035. <http://doi.org/10.1016/j.jmbbm.2021.105035>. PMID:34906864.
  8. Cerrutti BM, Zambon M, Megiatto DJR Jr, Frollini E. Synthesis of carboxymethylcelluloses with different degrees of substitution and their performance as renewable stabilizing agents for aqueous ceramic suspensions. *Ind Crops Prod*. 2017;107:54-62. <http://doi.org/10.1016/j.indcrop.2017.05.029>.
  9. Cerrutti BM, Lamas JC, Campana-Filho SP, Frollini E. Carboxymethyl chitosan: preparation and use in colloidal ceramic processing. *J Polym Environ*. 2021;21(3):816-25. <http://doi.org/10.1007/s10924-012-0566-7>.
  10. Cerrutti BM, Souza CS, Castellan A, Ruggiero R, Frollini E. Carboxymethyl lignin as stabilizing agent in aqueous ceramic suspensions. *Ind Crops Prod*. 2012;36(1):108-15. <http://doi.org/10.1016/j.indcrop.2011.08.015>.
  11. Wiśniewska M, Urban T, Grzadzka E, Zarko VI, Gun'ko VM. Comparison of adsorption affinity of polyacrylic acid for surfaces of mixed silica-alumina. *Colloid Polym Sci*. 2014;292(3):699-705. <http://doi.org/10.1007/s00396-013-3103-x>. PMID:24610970.
  12. Nan B, Olhero S, Pinho R, Vilarinho PM, Button TW, Ferreira JMF. Direct ink writing macroporous lead-free piezoelectric  $\text{Ba}_{0.85}\text{Ca}_{0.15}\text{Zr}_{0.1}\text{Ti}_{0.9}\text{O}_3$ . *J Am Ceram Soc*. 2018;102(6):3191-203. <http://doi.org/10.1111/jace.16220>.
  13. Schlördt T, Schwanke S, Keppner F, Fey T, Travitzky N, Greil P. Robocasting of alumina hollow filament lattice structures. *J Eur Ceram Soc*. 2013;33(15-16):3243-8. <http://doi.org/10.1016/j.jeurceramsoc.2013.06.001>.
  14. Baltazar J, Alves MFRP, Santos C, Olhero S. Reactive sintering of  $\text{Al}_2\text{O}_3$ - $\text{Y}_2\text{O}_3$ - $\text{Al}_2\text{O}_3$  ceramic composites obtained by direct ink writing. *Ceramics*. 2022;5(1):1-12. <http://doi.org/10.3390/ceramics5010001>.
  15. Santos C, Baltazar J, Alves MFRP, Olhero SM. Development of translucent zirconia by Robocasting. *Mater Lett*. 2022;325:132785. <http://doi.org/10.1016/j.matlet.2022.132785>.
  16. Santos C, Baltazar J, Alves MFRP, Olhero SM. Translucent zirconia dental prosthesis processed by Direct Ink Writing: updates and challenges. *J Manuf Process*. 2024;131:1656-66. <http://doi.org/10.1016/j.jmapro.2024.09.105>.
  17. Olhero SM, Torres PMC, Mesquita-Guimarães J, Baltazar J, Pinho-da-Cruz J, Gouveia PCS. Conventional versus additive manufacturing in the structural performance of dense alumina-zirconia ceramics: 20 years of research, challenges and future perspectives. *J Manuf Process*. 2022;77:838-79. <http://doi.org/10.1016/j.jmapro.2022.02.041>.
  18. Lévaro NRM, Alves MFRP, Santos S, Sencadas V, Olhero S. Direct ink writing of ATZ composites based on inks prepared by colloidal or hydrogel route: linking inks rheology with mechanical properties. *Colloids Surf A Physicochem Eng Asp*. 2023;668:131426. <http://doi.org/10.1016/j.colsurfa.2023.131426>.
  19. Du WB, Tatsuzawa K, Aizawa T, Kihara J. Processing and characterization of alumina wire by controlled fracture forming process: (II) resintering behavior and mechanical properties. *Mater Sci Eng A*. 2001;316(1-2):248-57. [http://doi.org/10.1016/S0921-5093\(01\)01242-4](http://doi.org/10.1016/S0921-5093(01)01242-4).
  20. Zhao J, Harmer MP. Effect of pore distribution on microstructure development: ii, first- and second-generation pores. *J Am Ceram Soc*. 1988;71(7):530-9. <http://doi.org/10.1111/j.1151-2916.1988.tb05916.x>.
  21. Zhao J, Harmer MP. Effect of pore distribution on microstructure development: III, model experiments. *J Am Ceram Soc*. 1992;75(4):830-43. <http://doi.org/10.1111/j.1151-2916.1992.tb04148.x>.
  22. Gregorová E, Pabst W, Nečina V, Uhlířová T, Diblíková P. Young's modulus evolution during heating, re-sintering and cooling of partially sintered alumina ceramics. *J Eur Ceram Soc*. 2019;39(5):1893-9. <http://doi.org/10.1016/j.jeurceramsoc.2019.01.005>.
  23. Du W-B, Tatsuzawa K, Aizawa T, Kihara J. Densification and resintering behavior of alumina compacts processed by controlled fracture forming. *J Jap Soc Powder Powder Metall*. 1998;45(4):326-9. <http://doi.org/10.2497/jjspm.45.326>.
  24. ASTM: American Society for Testing and Materials. ASTM B-962-17: standard test methods for density of compacted or sintered powder metallurgy (PM) products using archimedes' principle. West Conshohocken: ASTM International; 2017.
  25. Almatís. Global Product Data—CT 3000 LS SG [Internet]. 2021 [cited 2024 Jan 1]. Available from: [https://www.almatis.com/media/hamk2s0i/gp-rcp\\_024\\_ct3000ls\\_sg\\_0812.pdf](https://www.almatis.com/media/hamk2s0i/gp-rcp_024_ct3000ls_sg_0812.pdf)
  26. Casellas D, Ràfols I, Llanes L, Anglada M. Fracture toughness of zirconia-alumina composites. *Int J Refract Hard Met*. 1999;17(1):11-20. [http://doi.org/10.1016/S0263-4368\(98\)00064-X](http://doi.org/10.1016/S0263-4368(98)00064-X).
  27. Nascimento ACP, Coutinho MM, Alves MFRP, Santos C, Ferreira JLA, Silva CRM. Effect of addition of previously-synthesized Ce-TZP/ $\text{Al}_2\text{O}_3$  submicrometric powder on the properties of  $\text{Al}_2\text{O}_3$ -based ceramics. *Mater Res*. 2022;25:e20210510. <http://doi.org/10.1590/1980-5373-mr-2021-0510>.
  28. Hsu Y-F. Influence of  $\text{Nb}_2\text{O}_5$  additive on the densification and microstructural evolution of fine alumina powders. *Mater Sci Eng A*. 2005;399(1-2):232-7. <http://doi.org/10.1016/j.msea.2005.03.101>.
  29. Silva BM, Santos ÉMB, Souza VZB, Alves MFRP, Vieira CM, Santos C. Drying behaviour of  $\text{Al}_2\text{O}_3$  inks containing carboxymethylcellulose (CMC) for use in colloidal processing. *Ceramics*. 2023;6(2):935-47. <http://doi.org/10.3390/ceramics6020055>.
  30. Kowalski SJ. Thermomechanics of drying processes. Berlin: Springer; 2003.
  31. Schneider CA, Rasband WS, Eliceiri KW. NIH Image to ImageJ: 25 years of image analysis. *Nat Methods*. 2012;9(7):671-5. <http://doi.org/10.1038/nmeth.2089>. PMID:22930834.
  32. Galusek D, Twigg PC, Riley FL. Wet erosion of liquid phase sintered alumina. *Wear*. 1999;233-235:588-95. [http://doi.org/10.1016/S0043-1648\(99\)00236-7](http://doi.org/10.1016/S0043-1648(99)00236-7).
  33. Goh GKL, Lim LC, Rahman M, Lim SC. Effect of grain size on wear behaviour of alumina cutting tools. *Wear*. 1997;206(1-2):24-32. [http://doi.org/10.1016/S0043-1648\(97\)00002-1](http://doi.org/10.1016/S0043-1648(97)00002-1).
  34. Hsu YF, Wang SF, Wang YR, Chen SC. Effect of niobium doping on the densification and grain growth in alumina. *Ceram Int*. 2008;34(5):1183-7. <http://doi.org/10.1016/j.ceramint.2007.02.010>.
  35. Hossain SS, Lu K. Review - Recent progress of alumina ceramics by direct ink writing: ink design, printing and post-processing. *Ceram Int*. 2023;49(1):10199-212. <http://doi.org/10.1016/j.ceramint.2023.01.143>.